A new chemical pathway towards densification of tetragonal zirconia below 900°C

Maria Isabel Rua Taborda, Etienne Martin, U-Chan Chung, Sébastien Fourcade, Christine Labrugère, Dominique Michau, Graziella Goglio, Catherine Elissalde

A new chemical pathway towards densification of tetragonal zirconia below 900°C

M.I. Rua Taborda, E. Martin, U-C. Chung, S. Fourcade, C. Labrugère, D. Michau, G. Goglio and C. Elissalde*

Univ. Bordeaux, CNRS, Bordeaux INP, ICMCB, UMR 5026, F-33600 Pessac, France

*Corresponding author: catherine.elissalde@icmcb.cnrs.fr
ICMCB-CNRS, 87 avenue du Dr Albert Schweitzer, 33608 Pessac Cedex, France

The recent development of low temperature sintering approaches leads to promising perspectives in terms of global optimisation of functional materials and multi-materials. These new processes mobilize different densification mechanisms and offer a tremendous flexibility in terms of chemical reactivity. In this context, we focus here on the densification of yttria stabilized zirconia (3Y-ZrO_2) at a temperature below 900°C combining a transient chemical reactivity induced during the Cold Sintering Process with diffusion mechanisms activated during the Spark Plasma Sintering. The chemistry is tuned *in-situ* through the presence of a hydrated zirconium carbonate whose role at each stage of the whole process is discussed. Tetragonal 3Y-ZrO_2 nanostructured ceramics were thus densified up to 92-95% below 900°C.

Keywords: spark plasma sintering, cold sintering process, chemical reactivity, nanostructured zirconia ceramics, X-ray photoelectron spectroscopy

1. Introduction

Zirconia is a reference material due to the combination of specific properties which makes it suitable for a broad range of applications. Controlling the microstructure and structure in terms of grain size, porosity and stability of cristalline polymorphs, understanding the sintering mechanisms and lowering the sintering temperature remain challenges to further properties optimization. For this purpose and beyond conventional sintering, the benefits of advanced sintering techniques, such as Two Step Sintering [1] , Microwave-assisted Sintering [2], and Field Assisted Sintering (FAST) processes [3–5], have been clearly established. A reduction of sintering temperatures in the range of 1000 - 1400°C has thus been achieved. Focusing on Yttria-stabilized zirconia sintered by Spark Plasma Sintering (SPS), A. Flaireau *et al.* have recently reported a complete analysis of grain growth and

densification mechanisms according to the grain size and yttria content [6]. A possible overlapping of densification mechanisms by surface diffusion and grain boundary sliding accommodated by interface-reaction has been identified for nanometer grain size 3Y-ZrO_2. Furthermore, Cold Sintering Process (CSP), developped by C. Randall and collaborators, has brought new chemical pathways to drastically lower the sintering temperature of many materials and multimaterials, leading then to a clear paradigm shift for processing of ceramics [7–9]. In the case of yttria-stabilized zirconia, the CSP sintering temperature was as low as 180°C using water as transient solvent to assist this first step of densification [10,11]. However, to reach a density higher than 95% while stabilizing the tetragonal phase, a conventional post-annealing at 1100°C was necessary. Given the low solubility of zirconia in standard pH conditions, dissolution-precipitation mechanisms are hardly triggered. A different approach combining the chemical reactivity of zirconium hydroxide precursors with SPS was shown to be an efficient strategy for crystallisation and densification of nanocrystalline ZrO_2 at 350°C under pressure [12]. Here, the typical sequence of hydroxide transformation is involved when increasing the temperature, starting with the formation of an amorphous zirconia phase, which then crystallizes in a metastable tetragonal phase (300-400°C), and finally transforms into the thermodynamically stable monoclinic phase at higher temperature. Local atomic rearrangements (topotactic/martensitic transformations) are expected in the crystallisation/densification mechanism. A very cohesive nanostructure with a homogeneous distribution of meso/microporosity was obtained but optimal density and stabilization of the tetragonal polymorph were not yet reached.

The potential of advanced low temperature sintering processes to benefit of new mass transport pathways and chemical reactivity enhancement is obvious in order to activate the densification of zirconia at lower temperature. A key aspect is to efficiently adapt the chemistry through the suitable solvent or precursors. Note that alternatives to solvents, such as ionic eutectic molten salts or solvent-chelating agent mixtures, lead to efficient densification by CSP for many oxides including those with incongruent dissolution [13]. Although the CSP method does not systematically induce a direct densification, using it as a preliminary step has been demonstrated to be beneficial in the

reduction of both time and temperature of the overall sintering process. Indeed, the samples processed using Cold Sintering Process in a first step are densified in a second conventional step at much lower temperature than standard processing, and the microstructure can be controlled. This was demonstrated not only in the case of yttria stabilized zirconia but also in the case of various materials including lead free piezoceramics (KNN, CeO_2, $SrTiO_3$, $Li_2Mg_3TiO_6$, etc.) [14].

In the present work, the sintering profile includes a first CSP step in a specific temperature window defined by the thermal behaviour of a hydrated zirconium carbonate powder added to the zirconia nanopowder. The role of this carbonate is to provide *in situ* a reactive chemical pathway at the grain boundaries. No solvent is added to the initial powder but *in situ* dehydration of $(ZrO_2)_2CO_2*xH_2O$ is induced during CSP. The objective is thus to prepare by CSP a highly reactive green compact and to activate the densification by SPS at low temperature.

2. Characterizations of the zirconia powder and the hydrated zirconium carbonate

First, the investigations conducted on the two commercial precursors, 3Y-ZrO_2 (99.9%, 20nm purchased from US Research Nanomaterials, Inc.Houston, TX, USA) and amorphous hydrated zirconium carbonate ($(ZrO_2)_2CO_2*xH_2O$ (Alpha Aesar)), are presented. The 3Y-ZrO_2 powder was characterized by XRD, TEM and granulometry (Suppl. Inf. **Figure 1SI**). A ratio of phases close to 90% tetragonal and 10% mononoclinic was determined from Rietveld refinement of room temperature X-ray diffraction pattern. The grain size estimated by TEM corresponds to 19-20nm (Figure 1SI).

Thermal (DSC, TGA) and X-ray photoelectron spectroscopy (XPS) analyses of the zirconium carbonate were first performed in order to define the CSP temperature. Characterization procedures are detailed in the supporting information (SI). Thermogravimetric analysis of the zirconium carbonate shows the release of physisorbed water up to 150°C **(Figure 1a)**. The desorption of CO_2 being adsorbed at room temperature and trapped by the adsorbed water could also contribute at low temperature [15]. The chimisorbed water loss is observed in the range 150-500°C (**Figure 1a**), and the additional mass decrease at around 550°C is ascribed to the decomposition of the carbonate. Other compounds such as CO_3^{2-}-based species volatilize at higher temperatures during carbonate

decomposition and crystallization into ZrO_2. The DSC analysis shows a first endothermic peak associated with the first mass loss in TGA corresponding to dehydroxylation (**Figure 1b**). A second exothermic signature at T>450°C is ascribed to the cristallisation onset of the amorphous zirconium carbonate into metastable tetragonal zirconia. This is supported by XRD analyses performed after calcination of the hydrated zirconium carbonate at different temperatures *i.e.* 400 °C (amorphous phase), 500°C (tetragonal phase), 600°C and 700°C (monoclinic phase) (not shown). To further analyse the surface chemistry and probe the thermal stability of the zirconium carbonate, XPS analyses were carried out on the raw carbonate (unsteamed) and the carbonate steamed at 120°C. The XPS depth profiles and fitted C1s and O1s spectra of both samples are shown in **Figure 2SI and Figure 1 (c-d)**. The depth concentration profiles clearly show a decrease in carbon content of the steamed material (5 at% vs. 19 at%) (**Figure 2SI,** Table 1SI). The fit pattern of O1s goes through three components: O^{2-} bonds (ZrO_2) around 530.2 eV, OH and O=C around 531.7 eV and O-C around 532.7 eV (**Figure 1 (c-d)**). Note that at the extreme surface (0s etching), the OH component is particularly important on the unsteamed material while it drops significantly on the steamed one (**Figure 1 (c-d)** (right)). After etching (480s), which allows the extreme surface pollution to be eliminated, the component around 532.7 eV collapses. The two low energy components then give an indication of the OH/O^{2-} ratio corresponding to 54/100 and 29/100 for the unsteamed and steamed powder, respectively (see Table 1SI, area ratio of the two components normalized to 100 versus O^{2-}, details relative to the fit are given in SI). Concerning the C1s fits, the extreme surface spectra (0s etching) are quite similar, largely due to surface carbon pollution (**Figure 1 (c-d)** (left)). On the other hand, the sub-surface spectra (480s etching) have interesting signatures since they reveal the persistence of carbonate bonds through the component located around 290.2 eV. Note that for the 3Y-ZrO_2 initial powder, the C1s fit in depth does not reveal significant carbonate component; moreover, the surface O1s does not reflect an OH component as high as in zirconium carbonate powders (**Figure 3SI**). At a deeper level, the OH component remains with a ratio of OH/O^{2-}= 16/100 (**Table 1SI**).

3. Double step sintering approach

An amount of 3 wt% of amorphous zirconium carbonate was added to 1.5 grams of zirconia powder. The mixture was directly placed in the CSP mold (13mm diameter) without any solvent. Based on the different analyses of the zirconium carbonate, the dwell temperature of CSP was set at 110°C in order to release *in situ* the physisorbed water, to retain both chemisorbed water and carbonate species and to avoid cristallization into zirconia. A heating ramp of 10°C/min and a dwell of 150min were selected and the applied pressure was 350MPa (pressure being applied before heating and throughout the heat treatment). The solubility of zirconia is low even under high pressure conditions, but the chemistry triggered in situ by the dehydration and destabilisation of the zirconium carbonate required specific pressure and temperature conditions. The applied pressure of 350MPa is necessary to ensure sufficient mechanical cohesion to handle the CSP pellet directly in the SPS and also to promote particle rearrangement and compaction in order to limit large microstructural defects that would be difficult to remove in the second SPS step. Lower pressures were tested in the CSP step, but did not optimize the final densification. Reducing the sintering time for both the CSP and SPS stages is currently being investigated in order to smooth out the overall process conditions. Pressure will remain a much more difficult parameter to reduce. After CSP, the relative density is close to 55% indicating that no densification has been initiated. XPS analyses on fractured CSP sample reveal carbonate components in small quantities at sub-surface (figure 2). The surface O1s does not show any intense OH component but this component clearly remains at a deeper level with an OH/O^{2-} ratio estimated close to 10/100 (**Table 1SI**).

The CSP pellet was then introduced directly into the SPS set-up (Dr Sinter 515S, Syntex, Japan). The set-up was modified by adding ring shape graphite foils and felts of different thicknesses to adapt the SPS mold diameter (15 mm) to the CSP pellet (13 mm) and homogeneize the application of the pressure. The SPS cycle was set at 850°C (ramp 50°C/min) with a dwell of 90 minutes and applying 100MPa. These SPS conditions, previously optimized on the sintering of 3Y-ZrO_2 without carbonate

and using water as a solvent with or without adding a mineralizer (NaOH) during the first CSP step, have led to a maximum density after SPS of 85%. These SPS parameters were maintained when using the zirconium carbonate in order to highlight its impact towards densification enhancement.

The relative density of the ceramic after SPS was evaluated at 92% and 95% by geometric measurements and Archimedes method in ethanol, respectively. A content of tetragonal phase higher than 95% was determined by Rietveld analysis (**Figure 3**). The reproducibility of the two-step approach was confirmed for both density values and tetragonal phase content. SEM micrograph of the fracture of the combined CSP-SPS ceramic is shown in **Figure 4**. The microstructure reflects a low porosity level and appears to be globally homogeneous. Nethertheless, the SEM micrograph shown in **Figure 4** illustrates a specific zone where two populations of grain sizes can be identified. A majority of grains through the sample have a size that lies in the range 70 -100nm (also observed on the SEM micrograph on figure 5b), while few grains are larger with a size higher than 100nm (left part in figure 4). The latter were identified by EDX as pure zirconia while the more homogeneous and finer grains correspond to yttria zirconia. Whatever the grain size range, the grains are faceted and transgranular fracture appears to be the main fracture mode observed. For sake of comparaison and to highlight the benefit of the first CSP step with the addition of zirconium carbonate, the 3Y-ZrO_2 powder mixed with 3wt% amorphous hydrated zirconium carbonate was directly sintered by SPS at 850°C under 100MPa. The microstructural features of this sample (**Figure 5a**) can be compared with the microstructure of a combined CSP-SPS ceramic (**Figure 5b**). The level of porosity of the SPS ceramic is higher and corresponds to the low-density value obtained by Archimedes method (i.e. 70%). The morphology of the grains is significantly different, being rounded with an average grain size close to 50nm (**Figure 5a**).

The sintering conditions and associated microstructural features are reported and compared with those of various ZrO_2-3Y ceramics densified by different sintering processes in Table 1.

4. Discussion

The different investigations demonstrated that when zirconia is mixed with hydrated zirconium carbonate, the CSP step leads to a specific transient chemistry expected to enhance the reactivity of the system. A schematic showing the different steps involved in the sintering strategy and the associated possible mechanisms, is proposed on figure 6. The influence of thermal treatment on the chemistry and surface characteristics of simple basic zirconium carbonate have been investigated in several studies [21–23]. Surface properties were explored in particular for catalytic activities [24]. The hydrated carbonate exhibits a higher thermal stability considering that hydroxyl groups remain stable over a larger temperature range compared with the zirconium hydroxide, and contains also largest amount of acid-base sites [25]. Dehydration generated *in situ* during CSP allows to destabilize the carbonate through a transient reorganization while retaining chemisorbed water and carbonate species as shown by XPS. Such reactive species are expected to activate the densification at low temperature during SPS through the complete decomposition of the carbonate. This one is concomittent with the crystallisation of ZrO_2 which would favour a further stage of rearrangement and may also contribute to enhance chemical reactivity due to the mobility of ionic species such as CO_3^{2-} [26]. CO_2 -catalyzed sintering was reported for calcium oxide and the mechanisms investigated involve dissolution and chemisorption [22]. In this case, according to the sintering temperature and CO_2 partial pressure, coarsening by surface diffusion or densification by grain boundary diffusion is promoted [27]. The surface of zirconia contains acidic and basic groups (hydroxyl groups, $Zr^{4+}O^{2-}$ pairs) that can interact with CO_2 through the adsorption of HCO^{3-} and /or CO_3^{2-}, depending on the zirconia polymorph [17]. In the context of this work, the high mobility of surface ionic species can first contribute to the consolidation by surface ionic diffusion process. In addition, the specific graphitic environement of the SPS set-up (mold and felts) and the decomposition of the zirconium carbonate over a large temperature range both contribute to the low oxygen partial pressure during

sintering. The associated creation of oxygen vacancies can play a role in the stabilization of the tetragonal phase and can also favor a grain boundary diffusion pathway towards densification. A schematic of the different steps involved in the sintering strategy and the associated possible mechanisms is proposed on figure 6.

5. Conclusion

The recent progress in CSP and combined CSP approaches for ceramic sintering and microstructure control has clearly demonstrated the central role of the chemistry in the sintering mechanisms and transport pathways, offering a tremendous flexibility in terms of chemical reactivity. Chemistry is thus at the focal point of our strategy and the use of a carbonate active reagent associated to a combined CSP-SPS procedure was shown here to allow densification of tetragonal 3Y-ZrO_2 up to 92-95% below 900°C. The first CSP step seems to provide *in situ* a chemical environment (hydroxyls, carbonated species) suitable to trigger densification under the specific SPS sintering conditions with low oxygen partial pressure and at sufficiently low temperature. However, it remains difficult to clearly identify and decipher the complex mechanisms associated to densification and phase stabilization. Further work based on Electron Paramagnetic Resonance and impedance spectroscopies are in progress and would help to reach a better understanding of the defect chemistry and its key role on the densification mechanisms. Moreover, future optimizations aim at softening the sintering conditions. If the pressure remains an essential factor at this stage, ongoing studies targeting in particular the reduction of the sintering times are promising.

References:

[1] Mazaheri M, Simchi A, Golestani-Fard F. Densification and grain growth of nanocrystalline 3Y-TZP during two-step sintering. J Eur Ceram Soc 2008;28:2933–9. https://doi.org/10.1016/J.JEURCERAMSOC.2008.04.030.

[2] García-Gañán C, Meléndez-Martínez JJ, Gómez-García D, Domínguez-Rodríguez A. Microwave sintering of nanocrystalline Ytzp (3 Mol%). Journal of Materials Science 2006;41:5231–4. https://doi.org/10.1007/s10853-006-0433-9.

[3] Yang D, Raj R, Conrad H. Enhanced Sintering Rate of Zirconia (3Y-TZP) Through the Effect of a Weak dc Electric Field on Grain Growth. Journal of the American Ceramic Society 2010;93:2935–7. https://doi.org/https://doi.org/10.1111/j.1551-2916.2010.03905.x.

[4] Chintapalli R, Mestra A, García Marro F, Yan H, Reece M, Anglada M. Stability of Nanocrystalline Spark Plasma Sintered 3Y-TZP. Materials 2010;3:800–14. https://doi.org/10.3390/ma3020800.

[5] Cologna M, Rashkova B, Raj R. Flash Sintering of Nanograin Zirconia in <5 s at 850°C. Journal of the American Ceramic Society 2010;93:3556–9. https://doi.org/https://doi.org/10.1111/j.1551-2916.2010.04089.x.

[6] Flaureau A, Weibel A, Chevallier G, Estournès C. Study of the densification and grain growth mechanisms occurring during spark plasma sintering of different submicronic yttria-stabilized zirconia powders. J Eur Ceram Soc 2021;41:3581–94. https://doi.org/10.1016/J.JEURCERAMSOC.2021.01.032.

[7] Ndayishimiye A, Sengul MY, Sada T, Dursun S, Bang SH, Grady ZA, et al. Roadmap for densification in cold sintering: Chemical pathways. Open Ceramics 2020;2:100019. https://doi.org/10.1016/J.OCERAM.2020.100019.

[8] Sada T, Tsuji K, Ndayishimiye A, Fan Z, Fujioka Y, Randall CA. High permittivity BaTiO3 and BaTiO3-polymer nanocomposites enabled by cold sintering with a new transient chemistry: Ba(OH)2·8H2O. J Eur Ceram Soc 2021;41:409–17. https://doi.org/10.1016/J.JEURCERAMSOC.2020.07.070.

[9] Ndayishimiye A, Grady ZA, Tsuji K, Wang K, Bang SH, Randall CA. Thermosetting polymers in cold sintering: The fabrication of ZnO-polydimethylsiloxane composites. Journal of the American Ceramic Society 2020;103:3039–50. https://doi.org/https://doi.org/10.1111/jace.17009.

[10] Guo H, Bayer TJM, Guo J, Baker A, Randall CA. Current progress and perspectives of applying cold sintering process to ZrO_2-based ceramics. Scripta Materialia 2017;136:141–8. https://doi.org/10.1016/J.SCRIPTAMAT.2017.02.004.

[11] Guo H, Guo J, Baker A, Randall CA. Cold sintering process for ZrO_2-based ceramics: significantly enhanced densification evolution in yttria-doped ZrO_2. Journal of the American Ceramic Society 2017;100:491–5. https://doi.org/https://doi.org/10.1111/jace.14593.

[12] Elissalde C, Chung UC, Josse M, Goglio G, Suchomel MR, Majimel J, et al. Single-step sintering of zirconia ceramics using hydroxide precursors and Spark Plasma Sintering below 400 °C. Scripta Materialia 2019;168:134–8. https://doi.org/10.1016/J.SCRIPTAMAT.2019.04.037.

[13] Tsuji K, Ndayishimiye A, Lowum S, Floyd R, Wang K, Wetherington M, et al. Single step densification of high permittivity $BaTiO_3$ ceramics at 300 ^{o}C. J Eur Ceram Soc 2020;40:1280–4. https://doi.org/10.1016/J.JEURCERAMSOC.2019.12.022.

[14] Galotta A, Sglavo VM. The cold sintering process: A review on processing features, densification mechanisms and perspectives. J Eur Ceram Soc 2021;41:1–17. https://doi.org/10.1016/J.JEURCERAMSOC.2021.09.024.

[15] Gimblett FGR, Hussain A, Sing KSW. Thermal and related studies of some basic zirconium salts. Journal of Thermal Analysis 1988;34:1001–13. https://doi.org/10.1007/BF01913505.

[16] Dong J, Pouchly V, Biesuz M, Tyrpekl V, Vilémová M, Kermani M, et al. Thermally-insulated ultra-fast high temperature sintering (UHS) of zirconia: A master sintering curve analysis.

Scripta Materialia 2021;203:114076. https://doi.org/https://doi.org/10.1016/j.scriptamat.2021.114076.

[17] Hérisson de Beauvoir T, Ghomari Z, Chevallier G, Flaureau A, Weibel A, Elissalde C, et al. Flash Spark Plasma Sintering of 3YSZ: Modified sintering pathway and impact on grain boundary formation. J Eur Ceram Soc 2021;41:7762–70. https://doi.org/https://doi.org/10.1016/j.jeurceramsoc.2021.08.013.

[18] Zhang F, Spies BC, Vleugels J, Reveron H, Wesemann C, Müller W-D, et al. High-translucent yttria-stabilized zirconia ceramics are wear-resistant and antagonist-friendly. Dental Materials 2019;35:1776–90. https://doi.org/https://doi.org/10.1016/j.dental.2019.10.009.

[19] Ramesh S, Zulkifli N, Tan CY, Wong YH, Tarlochan F, Ramesh S, et al. Comparison between microwave and conventional sintering on the properties and microstructural evolution of tetragonal zirconia. Ceramics International 2018;44:8922–7. https://doi.org/https://doi.org/10.1016/j.ceramint.2018.02.086.

[20] Theenagaran S, Ting CH, Chin KL, Yeo WH, Ng CK, Ramesh S, et al. The Effects of Sintering Additives on the Sintering of 3Y-TZP Ceramic. IOP Conference Series: Materials Science and Engineering 2021;1117:12010. https://doi.org/10.1088/1757-899x/1117/1/012010.

[21] Gimblett FGR, Hussain A, Sing KSW. Influence of thermal treatment on the surface characteristics of basic zirconium carbonate and oxalate. Journal of Colloid and Interface Science 1988;125:619–26. https://doi.org/10.1016/0021-9797(88)90029-X.

[22] Ma M, Hou P, Cao J, Liu H, Yan X, Xu X, et al. Simple basic zirconium carbonate: low temperature catalysis for hydrogen transfer of biomass-derived carboxides. Green Chemistry 2019;21:5969–79. https://doi.org/10.1039/C9GC03033F.

[23] Pokrovski K, Jung KT, Bell AT. Investigation of CO and CO2 Adsorption on Tetragonal and Monoclinic Zirconia. Langmuir 2001;17:4297–303. https://doi.org/10.1021/la001723z.

[24] Son PA, Nishimura S, Ebitani K. Preparation of zirconium carbonate as water-tolerant solid base catalyst for glucose isomerization and one-pot synthesis of levulinic acid with solid acid catalyst. Reaction Kinetics, Mechanisms and Catalysis 2014;111:183–97. https://doi.org/10.1007/s11144-013-0642-6.

[25] Bachiller-Baeza B, Rodriguez-Ramos I, Guerrero-Ruiz A. Interaction of Carbon Dioxide with the Surface of Zirconia Polymorphs. Langmuir 1998;14:3556–64. https://doi.org/10.1021/la970856q.

[26] Ortali C, Julien I, Vandenhende M, Drouet C, Champion E. Consolidation of bone-like apatite bioceramics by spark plasma sintering of amorphous carbonated calcium phosphate at very low temperature. J Eur Ceram Soc 2018;38:2098–109. https://doi.org/10.1016/J.JEURCERAMSOC.2017.11.051.

[27] Maya JC, Chejne F, Bhatia SK. On the modeling of the co2-catalyzed sintering of calcium oxide. AIChE Journal 2017;63:3286–96. https://doi.org/https://doi.org/10.1002/aic.15696.

Initial particle size (nm)	Sintering Aids (%wt)	Pressure (MPa)	Dwel time (min)	Temperature or T_1/T_2 (°C) (two steps sintering)	Final Density (%)	Grain size (nm)	Process	Ref.
90	-	-	1 (Processing time)	1755	99	~178	TI-UHS	[16]
40	-	25	0	1620	92	< 350	Flash-SPS	[17]
40	-	-	120	1450	>99	~300	CS	[18]
20	-	-	5	1500	99	~360	CS	[19]
20	-	-	5	1300	99	~170	MW	[19]
75	-	-	1/1800	1300/1150	99	~110	CS/CS	[1]
20	-	100	10	1100	99	~125	SPS	[6]
-	0.5% MnO_2	-	1	1200	88	-	CS	[20]
20	30% H_2O	350/-	30/180	180/1100	95	~100	CSP/CS	[10,11]
20	**3% $(ZrO_2)_2CO_2*xH_2O$**	**100**	**90**	**850**	**70**	**~50**	**SPS**	
20	**3% $(ZrO_2)_2CO_2*xH_2O$**	**350/100**	**150/90**	**110/850**	**95**	**70-100**	**CSP/SPS**	

Table 1: A literature survey of ZrO_2-3Y ceramics sintered using different processes and conditions. In bold text the results of this study

a)

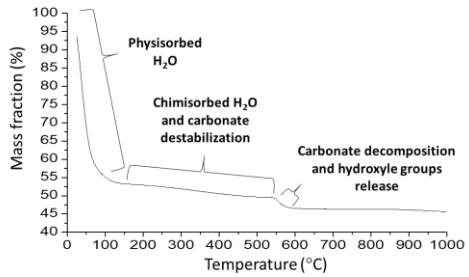

b)

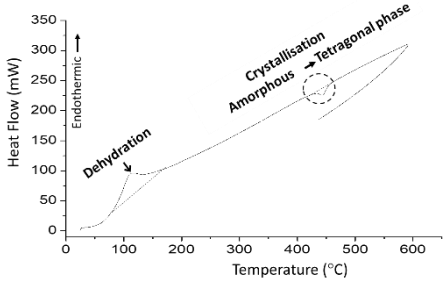

c)

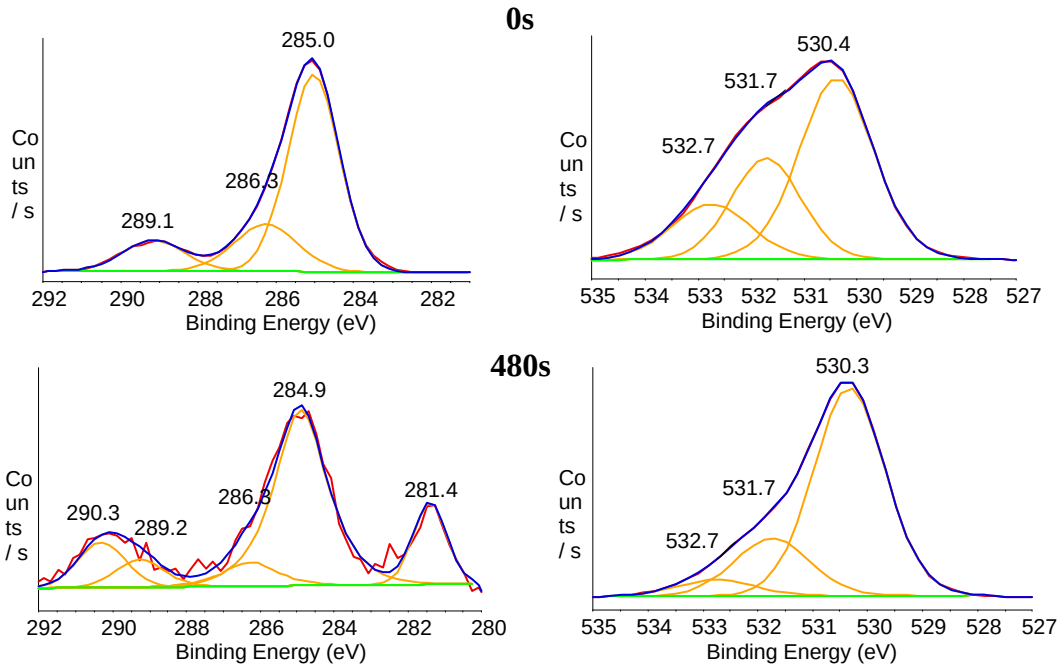

d)

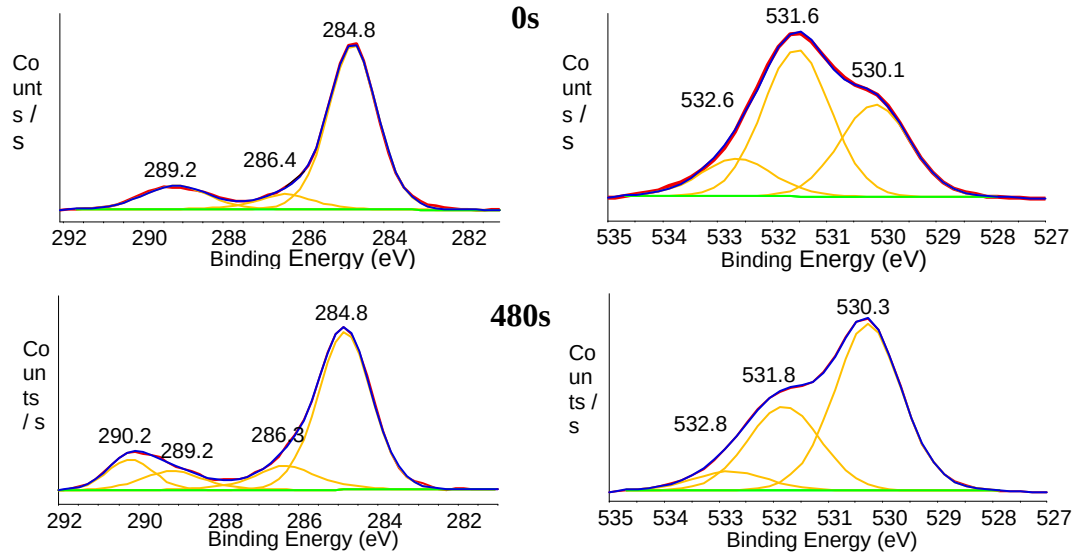

Figure 1 : a) TGA and b) DSC of the hydrated zirconium carbonate, XPS analyses : c) and d) fitted C1s (left) and O1s (right) spectra of hydrated zirconium carbonate c) unsteamed and d) steamed).

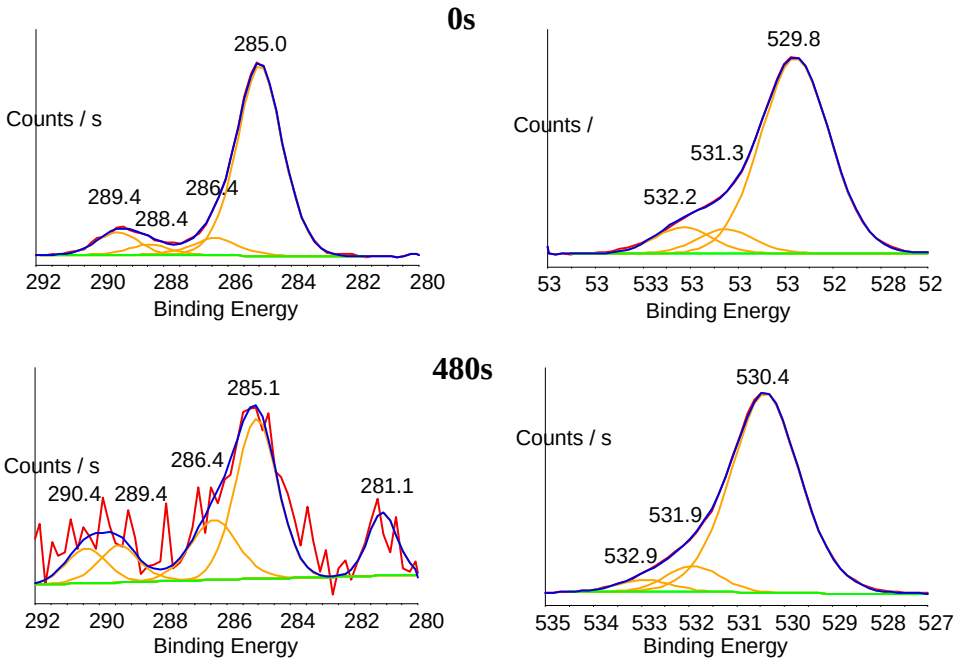

Figure 2 : Fitted C1s (left) and O1s (right) XPS spectra performed on sample after CSP (110°C - 150 minutes – 350MPa)

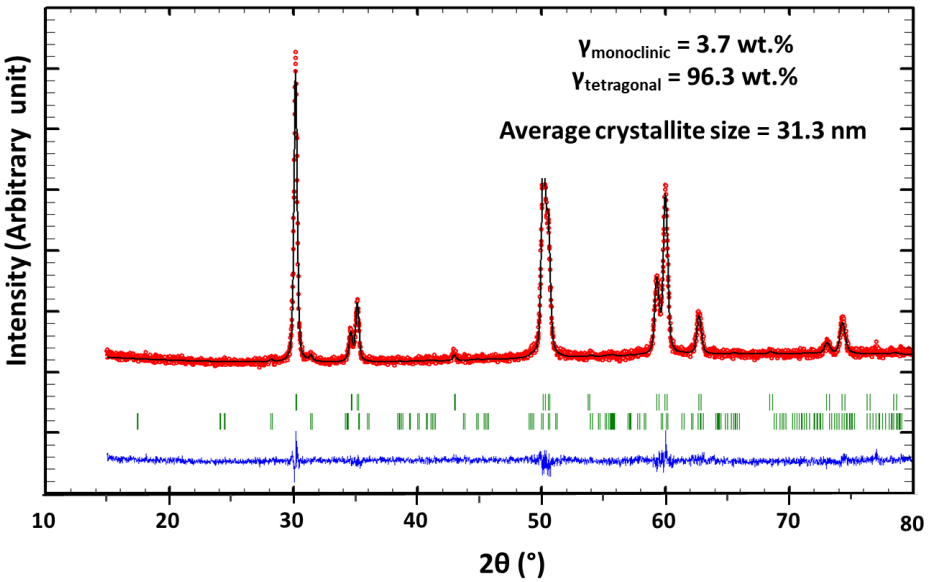

Figure 3 : Rietveld refinement of room temperature XRD pattern of 3Y-ZrO_2 ceramic processed by the combined CSP (110°C-150 minutes - 350MPa) and SPS (850°C- 90 minutes - 100MPa) approach using hydrated zirconium carbonate. The continuous black line, the red line, and the bottom blue line

represent the observed, calculated and difference patterns, respectively. The green vertical ticks represent Bragg positions of diffraction peaks in tetragonal 3Y-ZrO_2.

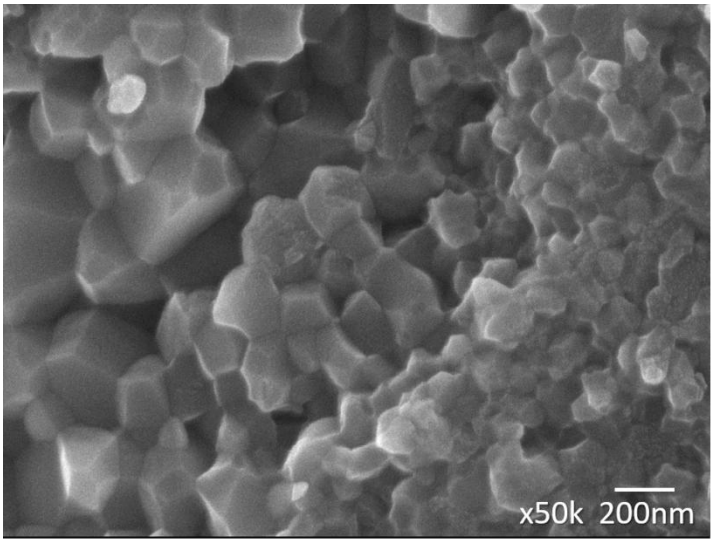

Figure 4 : HRSEM image of the fracture surface of the 3Y-ZrO_2 ceramics processed by the combined CSP (110°C-150 minutes - 350MPa) and SPS (850°C- 90 minutes - 100MPa) approach using hydrated zirconium carbonate.

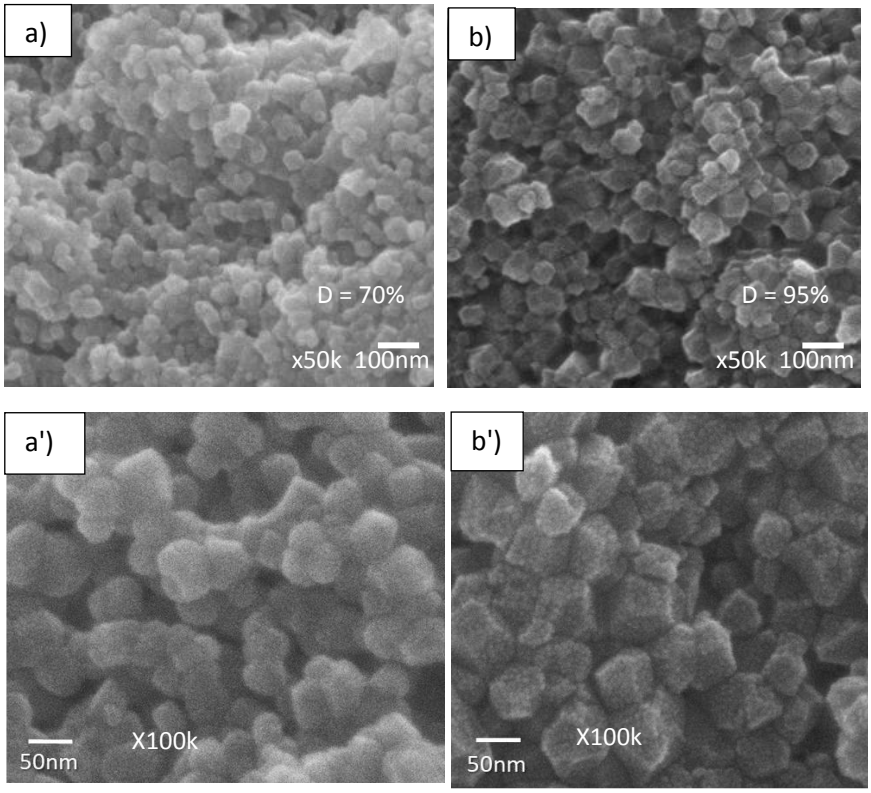

Figure 5 : HRSEM images of the fracture surface of the 3Y-ZrO_2 ceramics processed using hydrated zirconium carbonate a) and a') directly by SPS at 850°C and b) and b') by the combined CSP (110°C) and SPS (850°C) approach

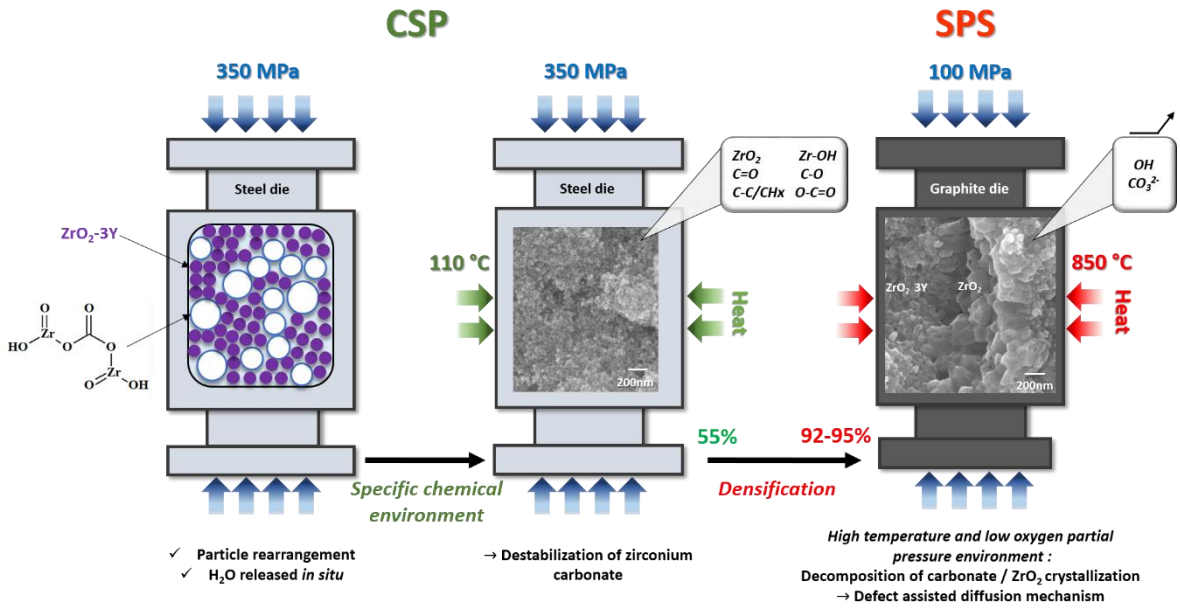

Figure 6 : Schematic of the different steps involved in the sintering strategy and the associated possible mechanisms.